Available online at www.sciencedirect.com

ScienceDirect

Physics Procedia 3 (2010) 1195–1200

Physics Procedia

www.elsevier.com/locate/procedia

14th International Conference on Narrow Gap Semiconductors and Systems

Room temperature interband cascade lasers

M. Kim, C. L. Canedy, C. S. Kim, W. W. Bewley, J. R. Lindle, J. Abell, I. Vurgaftman,* J. R. Meyer

Code 5613, Naval Research Laboratory, Washington, DC 20375

Abstract

An analysis of the threshold current densities and differential slope efficiencies in interband cascade lasers with type-II active regions revealed lower Auger recombination rates than anticipated theoretically or using the data from prior experiments. Furthermore, a new design of the waveguide yielded room-temperature internal losses as low as ≈6 cm^{-1}. The combination of these advances with improvements to the processing of narrow ridges has led operation up to 335 K in continuous-wave mode for devices emitting at 3.3-3.7 μm. An 8.7-μm-wide ridge without facet coatings produced up to 23 mW of cw power at 300 K, and displayed a maximum wall-plug efficiency of 2.0%.

Keywords: semiconductor lasers; mid-infrared lasers, interband cascade lasers.

1. Introduction

In spite of the major strides made recently by type-I antimonide quantum-well (QW) lasers [1],[2] and intersubband quantum cascade lasers (QCLs) [3],[4] at shorter and longer wavelength, respectively, there have been few continuous-wave (cw) coherent sources operating in the 3.0-4.4 μm mid-infrared (mid-IR) spectral window at ambient temperature. Such sources are needed in a wide variety of applications, from chemical sensing to infrared countermeasures. The most promising candidate to fill this gap is the type-II antimonide material system based on InAs electron wells and GaInSb hole wells [5]. Since the ohmic voltage drop of the laser circuit is appreciable on the scale of the mid-IR gap, and multiple QWs are generally needed to boost the optical gain, it is advantageous to employ the cascading geometry whereby the active QWs are connected in series (as in QCLs) rather in parallel (as in conventional QW lasers). The implementation of the resulting interband cascade laser (ICL) [6]-[8] is particularly convenient, since the semimetallic band alignment between InAs and GaSb allows the electrons that made a radiative transition to the valence band to be transferred readily back to the conduction band via elastic or nearly elastic processes.

Our group at NRL recently demonstrated the first ambient-temperature cw operation of an ICL, obtaining T_{max}^{cw} = 319 K at λ = 3.75 μm [9]. This achievement was made possible by the progress in both the MBE quality and the

* Corresponding author. Tel.: +1-202-404-8604; fax: +1-202-404-8114.
E-mail address: vurgaftman@nrl.navy.mil.

doi:10.1016/j.phpro.2010.01.162

Report Documentation Page

Form Approved
OMB No. 0704-0188

1. REPORT DATE	2. REPORT TYPE	3. DATES COVERED
2010		**00-00-2010 to 00-00-2010**

4. TITLE AND SUBTITLE	5a. CONTRACT NUMBER
Room temperature interband cascade lasers	5b. GRANT NUMBER
	5c. PROGRAM ELEMENT NUMBER
6. AUTHOR(S)	5d. PROJECT NUMBER
	5e. TASK NUMBER
	5f. WORK UNIT NUMBER
7. PERFORMING ORGANIZATION NAME(S) AND ADDRESS(ES) **Naval Research Laboratory,Code 5613,Washington,DC,20375**	8. PERFORMING ORGANIZATION REPORT NUMBER
9. SPONSORING/MONITORING AGENCY NAME(S) AND ADDRESS(ES)	10. SPONSOR/MONITOR'S ACRONYM(S)
	11. SPONSOR/MONITOR'S REPORT NUMBER(S)

12. DISTRIBUTION/AVAILABILITY STATEMENT
Approved for public release; distribution unlimited

13. SUPPLEMENTARY NOTES
14th International Conference on Narrow Gap Semiconductors and Systems, Sendai, Japan, 13th-17th July 2009.

14. ABSTRACT

15. SUBJECT TERMS

16. SECURITY CLASSIFICATION OF:			17. LIMITATION OF ABSTRACT	18. NUMBER OF PAGES	19a. NAME OF RESPONSIBLE PERSON
a. REPORT **unclassified**	b. ABSTRACT **unclassified**	c. THIS PAGE **unclassified**	**Same as Report (SAR)**	**6**	

level of understanding of the dominant optical and electronic mechanisms. Our theoretical modeling capability provides detailed simulations of the laboratory data, although this is often combined with empirical, trial-and-error variations of the relevant design parameters. In this paper, we describe some recent advances of the ICL development, and discuss factors that still limit the device performance.

2. Growth, processing, and pulsed characterization

The five-stage ($N = 5$) interband cascade lasers described in this work were grown on *n*-GaSb (100) substrates in a Riber Compact 21T MBE system, using methods described in Ref. [10]. The active region designs were generally similar to those described in Refs. [11] and [12], except for somewhat different thicknesses and compositions of the GaInSb hole wells and other relatively minor alterations. The *n*-type doping of the optical cladding layers was reduced from that in earlier 10-stage structures, in order to minimize internal losses. The designs of samples commencing with T080828 were further altered with the specific goal of reducing the internal loss.

In order to provide rapid feedback for wafer screening and design evaluation, standardized broad-area ridges of width 70-150 μm were produced by contact lithography and wet chemical etching for pulsed characterization. The etch proceeded to a GaSb separate-confinement layer below the active region. The mask set introduced intentional lateral corrugation of the ridge sidewalls, in order to frustrate parasitic lasing modes that can otherwise achieve feedback following strong reflections from the straight and deep-etched ridge boundaries. The broad-area devices were cleaved to a standard cavity length (L_{cav}) of 2 mm.

Narrow ridges for cw measurements were also processed from a few of the wafers. The ridges of width 4-10 μm were fabricated by photolithography and reactive-ion etching (RIE) using a Cl-based inductively-coupled plasma (ICP) process that again stopped at the GaSb SCL below the active QWs. The ridges were subsequently cleaned with a phosphoric-acid-based wet etch to minimize damage from the ICP RIE process. A 200-nm-thick Si_3N_4 dielectric layer was deposited by plasma-enhanced chemical vapor deposition, and a top contact window was etched back using SF_6-based ICP. Next, 100 nm of SiO_2 was sputtered to block occasional pinholes in the Si_3N_4. The ridges were metallized and electroplated with a 5-μm-thick heat-spreading layer of gold. Following the division into cavities guided by cleaving lanes in the electroplating, high-reflection (HR) or anti-reflection (AR) coatings were in some cases deposited on one or both facets. Each device was finally mounted epitaxial-side-up on a copper heat sink attached to the cold finger of an Air Products Heli-Tran Dewar.

The most reliable information about device characteristics, uncomplicated by lattice heating and the sidewall quality of narrow ridges, can be obtained by measuring the pulsed properties of broad-area lasers. In particular, the threshold current density j_{th} is inversely proportional to the carrier lifetime, whereas the differential slope efficiency dP/dI is related to the internal loss. However, in order to disentangle these quantities one also needs an estimate of the internal efficiency η_i, which expresses the fraction of the injected electrons that make the interband transition in the active region. While the physical processes that limit the internal efficiency in ICLs are not yet well understood, measurements as a function of cavity length [9],[13] can determine η_i (or at least set a lower bound if there is a pronounced dependence of the internal loss on cavity length, L_{cav}). For Sample T080227, η_i was found to decrease gradually with increasing temperature, from 83% at 78 K to 64% at 300 K [9]. As an approximation, we employ the same room-temperature internal efficiency for subsequent samples that were not measured as a function of L_{cav}. While this assumption affects the quantitative estimate for the internal loss, the derived Auger coefficient corresponding to the measured dP/dI and j_{th} is surprisingly insensitive to the value of η_i. We also note that a careful analysis of the facet reflectivity for well-confined TE-polarized modes [14] yields $R \approx 40\%$, whereas many previous studies used a value near 30%.

Figures 1 and 2 illustrate how the room-temperature threshold current densities and differential slope efficiencies of NRL ICLs have progressed over the last several years. The lowest j_{th} ever reported for a QCL (60 stages) [15] and that for an early non-cascaded type-II "W" laser [16] are also shown in Fig. 1. The initial drop in j_{th} for the 10-stage devices was associated with optimizing the active regions and doping profiles. The associated improvement in the internal loss, as reflected by the slope efficiencies of Fig. 2, were found to decrease the gains required to reach threshold to such an extent that j_{th} for the 5-stage ICLs became quite similar to those for the optimized 10-stage devices. Further design improvements that started with Sample T080828 then raised the differential slope efficiencies for 5-stage ICLs nearly to the level of earlier 10-stage devices. Although cavity-length studies have not

yet been performed on samples grown with the new design, an analysis of the slope efficiency data yields internal losses as low as 5.7 cm^{-1} (for T080828) at $T = 300$ K.

Auger coefficients γ_3 at $T = 300$ K, extracted by analyzing data such as those in Figs. 1 and 2, are shown in Fig. 3 for a large sampling of 3-, 5-, and 10-stage ICLs with a variety of active-region designs. The additional data for bulk and type-I QW materials, and for optically-pumped type-II structures, are taken mostly from Ref. [17]. Note first that the Auger coefficients determined for type-II QWs in ICLs are much lower than had been anticipated based on the earlier optically-pumped laser and photoconductivity experiments. This indicates that subsequent improvements in the MBE growth quality may have positively impacted the Auger coefficients, *e.g.*, via the elimination of defect- and/or interface-roughness-assisted processes. Also, the dependence on wavelength is much weaker than was implied by the earlier work. That the thicknesses and compositions of the GaInSb hole QWs were fixed in most of these samples appears to rule out any significant role for intervalence resonances that have drawn much theoretical attention [18]. The thresholds for devices emitting at the same λ, but with varying GaInSb thickness and composition were similar as well.

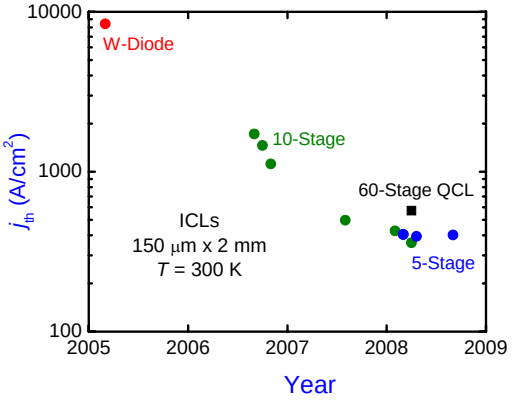

Fig. 1. Threshold current densities at 300 K for several 10-stage and 5-stage ICLs, as a function of the time when each wafer was grown. The lowest threshold reported for a QCL (with 60 stages) is also shown, along with that for an early "W" diode laser (non-cascade).

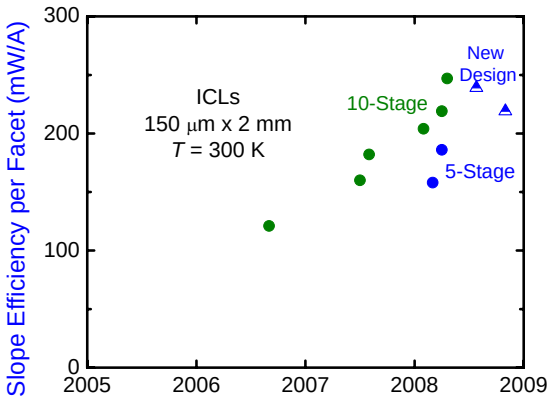

Fig. 2. Differential slope efficiency per facet at 300 K for several 10-stage and 5-stage ICLs *vs.* time when each wafer was grown.

The findings presented in Fig. 3 are highly beneficial to the prospects for high-temperature lasers operating in the 3.0-4.2 μm window. The observed γ_3 are 4-6 × 10^{-28} cm^6/s in this range, with any trends being weaker than the rather modest variations between samples. When λ is further increased to 4.5-5.0 μm, the derived Auger coefficients increase only slightly to 7 x 10^{-28} cm^6/s. The 3.4-4.2 μm range also corresponds to the highest slope efficiencies, *i.e.*, lowest internal losses. The slope efficiency decreases substantially at λ ≥ 4.5 μm, which may reflect stronger hole absorption in the active region and/or increased free-electron absorption in the separate-confinement and cladding regions. Curiously, the internal loss also increases at shorter wavelengths (≤ 3.4 μm), which may be due to some kind of defect-related parasitic absorption associated with the InAs/AlSb superlattice claddings. Further work is needed to map out the ultimate limits on the loss at those wavelengths.

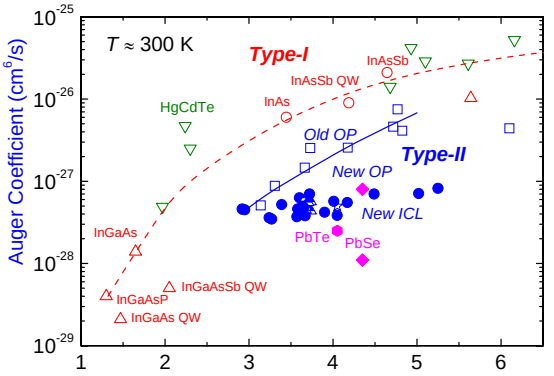

Fig. 3. Room-temperature Auger coefficient *vs.* laser emission wavelength or the effective wavelength corresponding to the energy gap of other devices, for a wide variety of pulsed, broad-area ICLs from this work and Ref. [12] (solid points), along with type-I and type-II data from Ref. [17] (open points). The lead salt data are from Refs. [19] and [20].

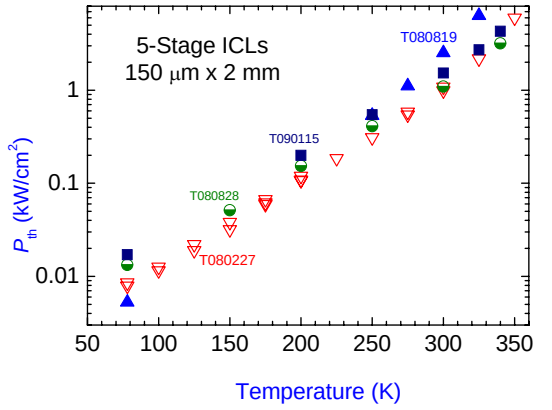

Fig. 4. Pulsed threshold power density *vs.* temperature for several of the representative laser samples discussed in the text.

The two primary figures of merit for achieving high-temperature cw operation are the threshold power density (P_{th}), which is obtained from the product of j_{th} and the bias voltage at threshold (V_{th}), and the rate of the threshold power density's increase above room temperature (*i.e.*, the characteristic temperature associated with P_{th}). The threshold voltage efficiency (defined as the ratio of the "useful" voltage drop $N\hbar\omega/q$ to V_{th}) of the best NRL ICLs to

date is ≈70-75%. Apart from the contribution on the order of k_BT per stage needed to overcome the internal loss, the remainder appears divided between an ohmic series resistance dropping over the substrate and the superlattice claddings and a non-ohmic part that may be associated with various band discontinuities in the structure. While the latter can probably be minimized further in the future, that will only incrementally improve P_{th}. In contrast, the best QCLs require an offset of multiple k_BT per stage for efficient carrier extraction from the lower lasing subband. The origin of the difference is primarily the large ratio between the lifetimes of upper and lower lasing states in interband active regions (where phonon scattering does not affect the former).

Figure 4 shows the threshold power density *vs.* temperature for several recent samples. The emission wavelengths at room temperature are 3.7 μm for T080227 and T080828, 4.5 μm for T080819, and 3.4 μm for T090115. At room temperature, the P_{th} for both samples emitting at $\lambda \approx 3.7$ μm are 1.1 kW/cm^2, which is close to the best value achieved for an ICL. P_{th} variations in the 1.0-1.6 kW/cm^2 range are observed for ICLs emitting at $\lambda = 3.0$-4.2 μm, which are driven roughly equally by changes in V_{th} and j_{th}, and some of which do not correlate with the laser design. Above $T = 300$ K, characteristic temperatures of 35-45 K are obtained for devices emitting near $\lambda = 3.7$ μm while the values are lower at longer wavelengths ($T_0 = 27$ K for Sample T080819). The relatively low values of T_0 observed in ICLs are consistent with a cubic dependence of the Auger rate on the carrier density (with a temperature-independent Auger coefficient). Therefore, further design optimization is likely to produce only incremental improvement to the characteristic temperature.

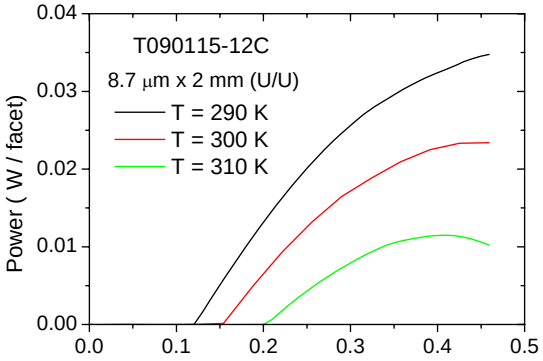

Fig. 5. CW output power per facet vs. current in Amps for an 8.7-μm-wide, 2-mm-long ridge with uncoated facets fabricated from Sample T090115.

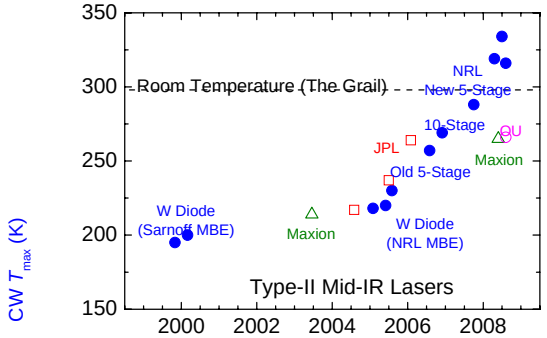

Fig. 6. Evolution of maximum CW operating temperature for interband lasers with type-II active regions emitting in the mid-IR spectral region.

3. CW results obtained with narrow-ridge devices

We previously reported that an ICL fabricated from T080227 operated in cw mode at λ = 3.75 μm up to a maximum temperature of 319 K [9]. Recent improvements in the etching of narrow ridges have led to maximum cw operating temperatures up to 335 K at λ = 3.7 μm (as well as T_{max} = 334 K at λ = 3.3 μm) [21]. Here we report the initial results of cw testing on narrow-ridge devices employing the new design, T090115. Figure 5 shows light-current characteristics at several temperatures for an 8.7-μm-wide ridge with L_{cav} = 2 mm and uncoated facets. Maximum cw output powers of 35 and 23 mW were observed for injection currents of 460 mA (j = 2.64 kA/cm^2) at T = 290 and 300 K, with the former value not yet saturated. The corresponding wall-plug efficiencies were 3.0 and 2.0%. A maximum operating temperature of 319 K was observed from a narrower 3.7-μm-wide ridge.

4. Conclusions

We have presented state-of-the-art performance characteristics for mid-IR interband cascade lasers. Figure 6 illustrates the evolution over the past decade of T_{max} in cw mode for different classes of interband type-II lasers. The steep slope over the past three years has resulted largely from optimizations enabled by the pulsed characterization detailed in Section 3. Further design improvements, particularly in the areas of threshold voltage and internal loss, appear possible, although the focus is likely to shift to the demonstration of high-power and single-mode ambient-temperature devices rather than further improvements to T_{max}. Room-temperature ICLs generating at least a few mW of cw power in a single spectral mode for any desired wavelength between 2.9 μm and about 4.5 μm should soon be available. Power scaling may take a little longer, since the small number of stages in optimized ICLs make them less suitable than QCLs for generating high powers from single narrow ridges without some other means (such as a tapered amplifier architecture) for increasing the active volume. The conclusions drawn in this paper will play an important role in determining the most promising avenues for future development.

References

1. L. Shterengas, G. Belenky, T. Hosoda, G. Kipshidze, and S. Suchalkin, Appl. Phys. Lett. 93 (2008) 011103.
2. T. Lehnhardt, M. Hümmer, K. Rössner, M. Müller, S. Höfling, and A. Forchel, Appl. Phys. Lett. 92 (2008) 183508.
3. Y. Bai, S. Slivken, S. R. Darvish, and M. Razeghi, Appl. Phys. Lett. 93 (2008) 021103.
4. M. Razeghi, A. Evans, Y. Bai, J. Nguyen, S. Slivken, S.R. Darvish, and K. Mi, Proc. Int. Conf. InP and Related Materials (Matsue Japan, 14 - 18 May 2007).
5. J. R. Meyer, C. A. Hoffman, F. J. Bartoli, and L. R. Ram-Mohan, Appl. Phys. Lett. 67 (1995) 757.
6. J. L. Bradshaw, J. D. Bruno, J. T. Pham, D. E. Wortman, S. Zhang, and S. R. J. Brueck, IEE Proc.-Optoelectron. 150 (2003) 288.
7. K. Mansour, Y. Qiu, C. J. Hill, A. Soibel, and R. Q. Yang, Electron. Lett. 42 (2006) 1034.
8. C. L. Canedy, C. S. Kim, M. Kim, D. C. Larrabee, J. A. Nolde, W. W. Bewley, I. Vurgaftman, and J. R. Meyer, J. Cryst. Growth 301 (2007) 931.
9. M. Kim, C. L. Canedy, W. W. Bewley, C. S. Kim, J. R. Lindle, J. Abell, I. Vurgaftman, and J. R. Meyer, Appl. Phys. Lett. 92 (2008) 191110.
10. C. L. Canedy, C. S. Kim, M. Kim, D. C. Larrabee, J. A. Nolde, W. W. Bewley, I. Vurgaftman, and J. R. Meyer, J. Vac. Sci. Technol. B 26 (2008) 1160.
11. C. L. Canedy, W. W. Bewley, J. R. Lindle, C. S. Kim, M. Kim, I. Vurgaftman, and J. R. Meyer, Appl. Phys. Lett. 88 (2006) 161103.
12. W. W. Bewley, J. R. Lindle, C. S. Kim, M. Kim, C. L. Canedy, I. Vurgaftman, and J. R. Meyer, Appl. Phys. Lett. 93 (2008) 041118.
13. W. W. Bewley, J. R. Lindle, C. L. Canedy, M. Kim, C. S. Kim, D. C. Larrabee, I. Vurgaftman, and J. R. Meyer, J. Appl. Phys. 103 (2008) 013114.
14. J. Buus, IEEE J. Quantum Electron. 17 (1981) 2256.
15. S. Katz, G. Boehm and M.-C. Amann, Electron. Lett. 44 (2008) 580.
16. C. L. Canedy, W. W. Bewley, J. R. Lindle, I. Vurgaftman, C. S. Kim, M. Kim, and J. R. Meyer, Appl. Phys. Lett. 86 (2005) 211105.
17. J. R. Meyer, C. L. Felix, W. W. Bewley, I. Vurgaftman, E. H. Aifer, L. J. Olafsen, J. R. Lindle, C. A. Hoffman, M. J. Yang, B. R. Bennett, B. V. Shanabrook, H. Lee, C. H. Lin, S. S. Pei, and R. H. Miles, Appl. Phys. Lett. 73 (1998) 2857.
18. C. H. Grein, M. E. Flatte, J. T. Olesberg, S. A. Anson, L. Zhang, and T. F. Boggess, J. Appl. Phys. 92 (2002) 7311.
19. R. Klann, T. Hofer, R. Buhleier, T. Elsaesser, and J. W. Tomm, *J. Appl. Phys.* **77**, 277 (1995).
20. P. C. Findlay, C. R. Pidgeon, R. Kotitschke, A. Hollingworth, B. N. Murdin, C. J. G. M. Langerak, A. F. G. van der Meer, C. M. Ciesla, J. Oswald, A. Homer, G. Springholz, and G. Bauer, *Phys. Rev. B* **58**, 12908 (1998).
21. I. Vurgaftman, C. L. Canedy, C. S. Kim, M. Kim, W. W. Bewley, J. R. Lindle, J. Abell, and J. R. Meyer, New J. Phys. (in press).